Environmental Earth Sciences (2018) 77:242
https://doi.org/10.1007/s12665-018-7417-3

THEMATIC ISSUE

Weathering assessment in the *Achala* Batholith of the *Sierra de Comechingones,* Córdoba, Central Argentina. III: appraising chemical weathering

J. O. Martínez[1] · V. A. Campodonico[1] · S. M. Formica[1] · P. J. Depetris[2]

Received: 12 September 2017 / Accepted: 12 March 2018 / Published online: 21 March 2018

Abstract
La Trucha is a small (~ 1.9 km^2), mountainous (~ 1300 m a.s.l.) granitic drainage basin, demonstrative of hundreds of second-order basins in the *Achala* Batholith of the *Sierras Pampeanas* of Córdoba, Argentina. Dominated by physical weathering and a *weathering-limited* denudation regime, the coarse- and fine-grained regolith has shown scant geochemical differences with the country rock. Erosion and sediment transport mainly occurs during torrential rain events (austral summer), whereas surface waters classify as *dilute* ($750 < T\Sigma^{+} < 375$ μeq L^{-1}) or *very dilute* ($375 < T\Sigma^{+} < 185$ μeq L^{-1}) water types. The dynamics of chemical weathering at *La Trucha* was approached through the use of major dissolved chemical components, comparing the performance of different methodologies in its assessment: mineral stability diagrams (i.e., chemical equilibria), the RE chemical weathering index, ternary diagrams, and PHREEQC inverse modeling. The latter approach allowed to probe into subtleties of the geochemical processes indicating that, besides the morphological dependency on mineral hydrolysis/dissolution or precipitation, there is a marked seasonal control that promotes or limits the occurrence of geochemical reactions.

Keywords Mountainous catchments · Low-order stream · Weathering signature · PHREEQC inverse modeling · Weathering-limited regime

Introduction

Increasing attention is being placed on mountainous rivers (e.g., Wohl 2010), partly because they are relatively less impacted by development than their lowland counterparts and, hence, natural processes can be examined in more detail, relatively free from human influence. Moreover, mountainous rivers are the "water towers of the world" and, therefore, it is particularly important the thorough understanding of all the complex aspects of their hydrological, geological/geochemical and biological functioning.

Mechanical and biological weathering usually precedes and facilitates the chemical hydrolysis of silicates in bedrocks or in the overlying regolith. The assessment of weathering intensity is achieved by calculating relative material losses (or gains) in the mineral debris. This is accomplished by means of a variety of approaches that include the calculation of indices, such as the Chemical Index of Alteration (CIA) (e.g., Nesbitt and Young 1982), the Chemical Index of Weathering (CIW) (Harnois 1988), the weathering index of Parker (WIP) (Hamdan and Burnham 1996) or, alternatively by a "benchmark mineral method" (e.g., Bland and Rolls 1998). In the case of *weathering-limited regimes* (Carson and Kirkby 1972)—as it happens in Argentina's *Sierras de Comechingones*, where the weathered material is removed more rapidly than it is generated—little regolith develops, and the debris derived from the source areas is partly unaffected. Under such circumstances, it is convenient to approach weathering intensity by revising the resulting dissolved phases in the water of streams and ground water.

This article is a part of Topical Collection in Environmental Earth Sciences on IV RAGSU—Advances in Geochemistry of the Surface in Argentina, edited by Dr. Americo Iadran Torres and Dr. Pablo Jose Bouza.

✉ J. O. Martínez
jomartinez@unc.edu.ar

[1] Centro de Investigaciones en Ciencias de la Tierra (CICTERRA), CONICET-Universidad Nacional de Córdoba, Avenida Vélez Sarsfield 1611, X5016DGA Córdoba, Argentina

[2] Academia Nacional de Ciencias, Avenida Vélez Sarsfield 229-249, X5000WAA Córdoba, Argentina

Hence, through this alternative pathway, seek to approximate the magnitude of mineral losses.

A year-long geochemical investigation was carried out in a small (~ 1.9 km^2) mountainous granitic watershed (known as *La Trucha*) located in the *Achala* Batholith (*Sierra de Comechingones*), in Central Argentina. The first part of the study included the assessment of the granite-regolith fractionation (Campodonico et al. 2014). A *weathering-limited regime* was recognized in the region, where denudation has been dominated by physical processes that occurred at a slower rate than erosion, with incipient chemical alteration. Chemical mass balance calculations performed between unaltered granite and two varieties of regoliths (i.e., coarse- and fine-grained), indicated that there were no statistically significant variations in any of the major, trace or rare earth elements in the coarser fraction, whereas statistically significant deficits of MgO, MnO, and P_2O_5 were recognized in the fine-grained regolith. These depletions were ascribed to initial alteration of biotite and apatite; plagioclase hydrolysis was clear through microscopic inspection (Campodonico et al. 2014).

The second part of the study (Martínez et al. 2016) showed that water chemistry is typical of streams draining F-rich granites, with high (austral) summer atmospheric precipitation determining the dilution of most major ions, with the exception of Cl^- that increases its concentration during high rainfall events. Rainfall-stimulated mobilization of K^+ is probably hidden by its affinity for adsorption onto fine-grained particles and that of SiO_2 by its biological consumption (e.g., Oliva et al. 2003; Frings et al. 2015). PHREEQC-calculated free CO_2 allowed the estimation of a mean carbon efflux of ~ 180 mg C m^{-2} $year^{-1}$ at *La Trucha* catchment, inferring that the first- and second-order streams of the *Achala* Batholith, which occupy an area of ~ 62.5 km^2, are significant sources in the *Sierra de Comechingones* carbon cycle.

In this third contribution to the ensuing experimental study on the characteristics of weathering in a small semiarid granitic catchment (i.e., *La Trucha* stream), the emphasis is placed on presenting additional geochemical characteristics and approaching weathering intensity through different pathways, including the calculation of indices and PHREEQC inverse modeling.

Study area

The small investigated catchment (~ 1.9 km^2) known as *La Trucha* (Spanish for "The Trout") is located in the *Achala* Batholith, in the southern sector of the *Sierra de Comechingones*, Córdoba, Argentina (31°54′07″S, 64°45′28″W; 31°53′11″S, 64°44′16″W) (Fig. 1). Bornhardts and relatively flat or gently undulating terrain are dominating features above 1000 m elevation in the *Sierra de Comechingones.*

Geology

The present-day high *sierra* uplifted by means of reverse faulting during the Cenozoic Andean orogeny (e.g., Isacks 1988). The range's western side has a steep slope (means of ~ 10%), whereas mean slopes are ~ 5% on the eastern side (e.g., Lecomte et al. 2009).

Early Cambrian middle to high-grade metamorphic rocks and Cambrian and Devonian granites prevail in the region (e.g., Siegesmund et al. 2010). These basement rocks are partially covered by unconsolidated Early Cenozoic sediments (e.g., Bonalumi et al. 1998). The massive intrusive body has a surface area of ~ 2500 km^2 and is discordant to structural features and to early Paleozoic igneous and metamorphic rocks. These Late Devonian granites have been characterized as aluminous A-type granites by Rapela et al. (2008) and their SiO_2 contents range between 60 and 76%.

The dominant facies (Facies B) in the *Achala* Batholith was identified as the main petrofacies in the drainage basin. It is a porphyritic monzogranite with K-feldspar megacrysts, plagioclase, biotite, and muscovite. Apatite, rutile, zircon, and opaque minerals were identified as accessory minerals, whereas clay minerals, chlorite, sericite, and muscovite occur as secondary phases (Lira and Kirschbaum 1990). A more comprehensive geological, morphological, and petrologic description has been incorporated by Campodonico et al. (2014).

Climate

The area of study lies in Argentina's temperate zone and the regional climate is continental, with unevenly spread atmospheric precipitations. Rainfall occurs typically during the (southern) summer and early autumn (about 75% of the total annual precipitation occurs between November and March), mainly due to humid air masses coming in from the north. The historical annual rainfall reaches a mean of ~ 1000 mm. Snowfall is scarce and mostly occurs during the late fall-early winter. The study area is characterized by an annual mean isotherm of 16 °C, dropping to about 10 °C at 2000 m elevation (Capitanelli 1979). The statistical analysis of recent rainfall and runoff data series in Central Argentina shows a significant positive trend in rainfall since the second half of the twentieth century. South of 31°S, spectral analysis shows the weak effect of El Niño-Southern Oscillation (ENSO) (Pasquini et al. 2006).

During the sampling period (March 2005–February 2006), rainfall was above the historical mean during the rainy season (austral summer) and was below the mean during the dry season (austral winter). Although there was a

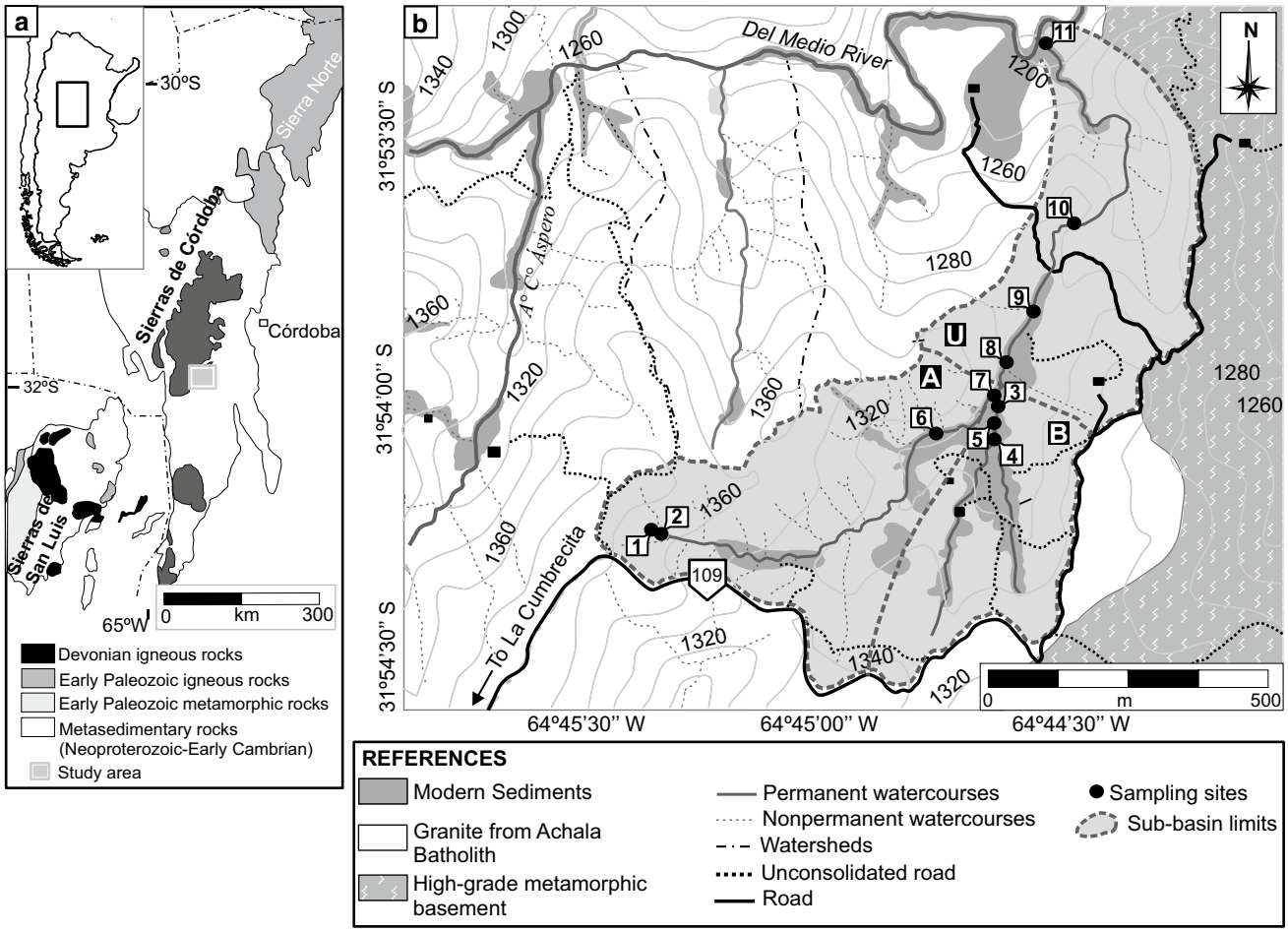

Fig. 1 **a** Location of the study area in (modified from Siegesmund et al. 2010). **b** Schematic topographical and geological map of *La Trucha* drainage basin, showing the location of sampling sites (modified from Campodonico et al. 2014; Martínez et al. 2016)

change in rainfall distribution throughout the year, the total annual precipitation (1078 mm) was close to the historical regional mean (1099 mm).

The *La Trucha* catchment

The small *La Trucha* catchment represents one of the hundreds of first- and second-order streams (e.g., Horton 1945; Strahler 1952) that drain the uppermost catchments of the *Achala* Batholith, in the *Sierras Pampeanas* of Argentina. This second-order catchment has a surface area of 1.9 km^2, a perimeter of 7.4 km, and its drainage network is markedly controlled by the fracture pattern of the batholith.

The maximum elevation in the catchment is 1374 m a.s.l. The main channel is ~ 3500 m long and reaches its outfall in the *del Medio* River at an elevation of 1207 m a.s.l. The overall mean slope is ~ 5% although the lowermost stretches are considerably steeper (~ 25%). The structural control determines that the western branch of the uppermost stretch is considerably steeper (~ 15%) than the eastern one (~ 7%). A more detailed morphological description of the *La Trucha* catchment has been included elsewhere (Martínez et al. 2016).

Materials and methods

Field and laboratory determinations

Surface water samples were collected in the studied drainage basin at 11 sampling stations (Fig. 1) between March 2005 and February 2006, in order to characterize the temporal and spatial variability of the total exported load. Field parameters (pH, electrical conductivity, total dissolved solids, temperature, dissolved oxygen and alkalinity) were determined using standardized methods (Eaton et al. 1995). Water samples were filtered through 0.22 µm cellulose acetate membrane filters (EMD Millipore, Billerica, MA, USA) and divided into two aliquots. The filtration equipment was rinsed repeatedly with sample water prior to filtration.

Aliquots used for the determinations of major cations and trace elements were acidified to pH < 2 with ultrapure HNO3 (> 99.999%, redistilled, Sigma–Aldrich Corp.) and stored in pre-cleaned polyethylene bottles. The other aliquot, used for the determination of major anions, was stored at 4 °C in pre-cleaned polyethylene bottles, without the acidification. Major anions (NO_3^-, F^-, Br^-, Cl^-, SO_4^{2-}, PO_4^{3-}) were measured using chemically suppressed ion chromatography with conductivity detection, whereas major cations and trace elements were determined by ICP-MS (Perkin Elmer Sciex Elan 6000—quadrupole mass spectrometer) at Activation Laboratories Ltd. (ActLabs, Ontario, Canada). Other details on the sampling strategy, and the analytical methodologies, have been described in earlier contributions on diverse aspects of weathering dynamics at the *La Trucha* watershed (Campodonico et al. 2014; Martínez et al. 2016).

Geochemical modeling

Chemical data were processed with AQUACHEM (Waterloo Hydrogeologic, Inc.) and PHREEQC (Parkhurst and Appelo 2013) softwares. These programs were employed to simulate silicate dissolution by means of inverse modeling. The inverse approach allows inferring the chemical reactions that occur when two or more water samples of known chemical composition react with a rock whose mineralogy is known. To do this, the model reconstructs all possible combinations of dissolution and/or precipitation reactions that explain the chemical changes observed between the two solutions and the mineral phases.

To analyze the chemical evolution of waters from *La Trucha* drainage basin, the climatic aspects, the differences in slopes and their relationship with water dynamics were considered. The four models defined in this study are shown in Fig. 2. Model 1 represents the transition from rainfall to the surface waters of the headwaters, model 2 comprises the upper basin, where slopes are ~ 5%, model 3 corresponds to the middle stretch of the river (slopes of ~ 2%), and model 4 comprises the lower basin until its outfall at the del Medio River (slopes of ~ 7%). The models were run with samples collected in June and March, corresponding to the dry and wet seasons, respectively.

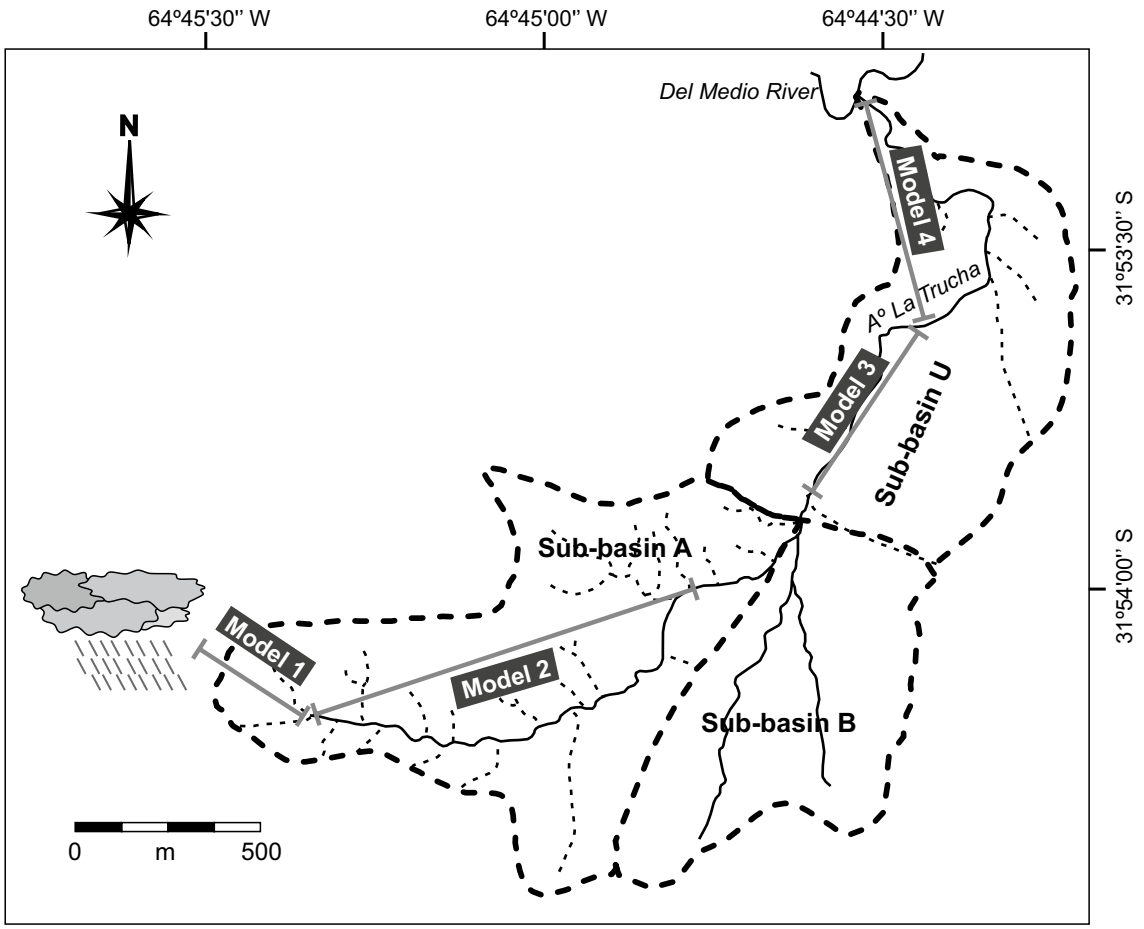

Fig. 2 Map of *La Trucha* drainage basin showing the inverse models performed with PHREEQC

The pH, temperature, major ion concentration and SiO_2 content of the solutions were needed to perform the geochemical modeling. PHREEQC also requires the definition of the uncertainties of each element and of the initial and final solutions. Different models were run for each stretch for both seasons (i.e., wet and dry) until the software parameters that best fitted the geology of the basin and the water chemistry were achieved. Table 1 summarizes the number of models obtained in each simulation, as well as the ones selected and the corresponding uncertainties which are given by the software. The criteria adopted to select the best model of each run was, basically, to choose the one that had the lowest uncertainty along with the largest number of mineral phases recognized in the petrological analysis carried out by Campodonico et al. (2014) in the watershed and included all the secondary minerals (kaolinite and illite) that were likely produced by incongruent weathering reactions.

Table 2 details the mineral phases used as possible sources and sinks of chemical species, which were selected taking into account the mineralogy of the *Achala* Batholith in this region (Lira and Kirschbaum 1990; Campodonico et al. 2014; Dahlquist et al. 2014). The plagioclase chosen for modeling purposes was oligoclase (Lira and Kirschbaum 1990; Lecomte et al. 2005). The dissolved F^- of the solutions was considered to be supplied by biotite, which usually includes fluoride in its octahedral sites (e.g., Li et al. 2003). The empirical formula of this mineral (Table 2) was obtained based on chemical analysis performed on biotites of the *Achala* Batholith, with F^- contents of 1.5% (Dahlquist et al. 2014). Therefore, the thermodynamic database of the software was modified in order to incorporate the alteration of fluorine-containing biotite. As the obtained simulations could not explain all the dissolved F^-, fluorite, a mineral described in the *Achala* Batholith (Lira and Kirschbaum 1990), was also involved as an alternative F^- source. Fluorapatite was not taken into account in the models as the dissolved concentration of PO_4^{3-} in *La Trucha* waters did not justify its addition.

Table 2 Theoretical composition of the mineral phases used in the inverse models

Phases	Formula
Biotite	$KMg_3AlSi_3O_{10}(OH)_{1.6}F_{0.4}$
Carbon dioxide	CO_2 (g)
Fluorite	CaF_2
Gypsum	$CaSO_4\ 2H_2O$
Illite	$K_{0.6}Mg_{0.25}Al_{2.3}Si_{3.5}O_{10}(OH)_2$
Kaolinite	$Al_2Si_2O_5(OH)_4$
K-feldspar	$KAlSi_3O_8$
K-mica	$KAl_3Si_3O_8(OH)_2$
Oligoclase	$Na_2Ca_{0.5}Al_3Si_7O_{20}$
Calcite	$CaCO_3$
Pure water	H_2O
Halite	NaCl

Calcite was considered as a possible reacting phase because the dissolved calcium is partly supplied by the dissolution of $CaCO_3$ present in soils and loess-like sediments (Pasquini et al. 2004). Such sediments in the mountainous area have shown calcite abundances of up to 10% (Pasquini et al. 2017; Rouzaut and Orgeira 2017). Other loess samples from the Chaco-Pampean plain in Argentina exhibited ~ 3% of $CaCO_3$ (Nicolli et al. 2010). Kaolinite and illite were chosen as precipitation facies, as they are the most common alteration products identified in these rocks (Campodonico et al. 2014). CO_2 was included as a gaseous phase since it participates in most weathering reactions, as well as in photosynthesis and respiration processes. Pure water was incorporated as an additional phase to simulate evaporation or dilution.

Table 1 Summary of inverse models exercises for *La Trucha* drainage basin performed with PHREEQC

Run	Solution		Uncertainty		Obtained models	Selected model
	Initial	Final	Initial	Final		
1	LL-LR2-K	JA4-1	0.150	0.025	2	Model 1_{Jun}
2	JA4-1	JA4-6	0.025	0.035	2	Model 2_{Jun}
3	JA4-8	JA4-10	0.030	0.065	1	Model 3_{Jun}
4	JA4-10	JA4-11	0.070	0.055	1	Model 4_{Jun}
5	LL-LR2-K	JA1-1	0.150	0.060	2	Model 1_{Mar}
6	JA1-1	JA1-6	0.045	0.060	1	Model 2_{Mar}
7	JA1-8	JA1-10	0.045	0.050	3	Model 3_{Mar}
8	JA1-10	JA1-11	0.035	0.065	2	Model 4_{Mar}

Results and discussion

Revisiting the main hydrochemical characteristics

The main chemical characteristics of *La Trucha*'s surface waters are shown in an earlier contribution (Martínez et al. 2016). However, it is deemed necessary to review the most outstanding features to facilitate the analysis that follows.

The mean electrical conductivity (± S.D.) in the system's stream waters were 49.95 ± 10.21 µS cm^{-1}, whereas the mean total dissolved solids (± S.D.) were 24.92 ± 5.14 mg L^{-1}. All water samples were almost neutral or slightly alkaline with a mean pH (± S.D.) of 7.24 ± 0.79. The mean alkalinity (± S.D.) determined in surface water samples was 349.67 ± 70.22 µeq L^{-1}, and it is mostly accounted for HCO_3^- concentrations in as much pH seldom exceeded 8.23.

Atmospheric precipitations played a major role in the control of specific electrical conductivity (and total dissolved solids), and alkalinity because, due to dilution, the lowest values were measured during the wet season. Summer rainfall determined neutral or faintly acid pH, whereas alkalinity increased during the dry season. Na^+ and Ca^{2+}, and HCO_3^- and F^- dominated about 89% of the total concentration of major cations and 90% of the total concentration of major anions. All the analyzed waters were of the HCO_3^- -type and fluctuated between the $Na^+ - K^+$-type, and the $Na^+ - K^+ - Ca^{2+}$-type.

According to the total sum of cations ($T\Sigma^+ = Na^+ + K^+ + 2\,Mg^{2+} + 2Ca^{2+}$), surface waters of *La Trucha* classify as *dilute* ($750 < T\Sigma^+ < 375$ µeq L^{-1}) or *very dilute* ($375 < T\Sigma^+ < 185$ µeq L^{-1}) water types in Meybeck's (2005) idealized model of fresh water chemistry.

The analysis on the likely sources of major dissolved components has been dealt with in an earlier contribution and the interested reader should refer to the relevant article (Martínez et al. 2016).

Chemical equilibria

The mineral stability diagrams are based on the incongruent solution of certain aluminosilicate minerals of igneous and metamorphic rocks. These reactions contribute to chemical weathering and result in the formation of oxides, hydroxides, clay minerals, or zeolites depending on the geochemical environment. The reactions that occur not only affect the solids but also the chemical composition of surface and ground water. The theoretical basis for these diagrams is provided by the Law of Mass Action and by the relationship between the standard free energy change of a chemical reaction and its equilibrium constant at 25 °C (Faure 1998).

The hydrolysis of feldspars, which are rapidly altered during the initial stages of weathering, produces kaolinite, whereas illite and smectite are intermediate products. The reactions involved in these transformations are used to construct the mineral stability diagrams, which also include other crystalline or amorphous minerals that can occur in the system.

The stability diagrams using the major cations Na^+, K^+, Ca^{2+} and Mg^{2+} of surface waters in *La Trucha* catchment were developed using AQUACHEM. In all cases, the distribution of samples in the stability diagrams is in concordance with the saturation indices given by geochemical modeling. The stability diagram for the system K_2O–Al_2O_3–SiO_2–H_2O (Fig. 3a, b) shows that samples cluster along a vertical line, within the field of kaolinite, with a trend toward the stability field of illite, mainly during the wet season (Fig. 3a). The samples that fall within the illite stability field correspond to the main channel (sub-basin U), downstream the confluence of the first-order tributaries A and B (Fig. 3b). Besides, most samples are close to the stability limit with montmorillonite (Fig. 3a, b). The vertical trend displayed by the samples, without important changes in the silicic acid, is better explained by the conversion of muscovite to kaolinite rather than by the hydrolysis of K-feldspar. Thus, the main source of K^+ is probably muscovite, which liberates K^+, consumes H^+, and does not incorporate H_4SiO_4 to the solution during its conversion to kaolinite.

In the case of the system Na_2O–Al_2O_3–SiO_2–H_2O (Fig. 3c, d), samples also plot in the kaolinite stability field, and a greater heterogeneity is observed during the wet season when the concentration of Na^+ increases (Fig. 3c). Samples of the main channel (sub-basin U) downstream the confluence of tributaries A and B are close to the Na-beidellite field (Fig. 3d). The chemical signature of waters after the confluence resembles that of the sub-basin B, which exhibits higher contents of H_4SiO_4 and Na^+ when compared to the rest of the samples.

The stability diagrams for the system CaO–Al_2O_3–SiO_2–H_2O (Fig. 3e, f) show that kaolinite and, to a lesser extent Ca-beidellite, are stable with the dissolved phase, being the Ca-beidellite more stable during the wet season. Besides, waters of the B branch and of the main channel after the confluence of both tributaries plot mainly in the Ca-beidellite stability field (Fig. 3f), reflecting the chemical signature of sub-basin B.

Finally, the system MgO–Al_2O_3–SiO_2–H_2O (Fig. 3g, h) shows that all samples have overcome the dissolved silica (H_4SiO_4) limit, which implies that waters are saturated with respect to quartz, but they have not reached the amorphous silica stability field. Samples of the main channel (sub-basin U) downstream the confluence of tributaries A and B fall within the talc stability field, mainly during the wet season (Fig. 3g, h).

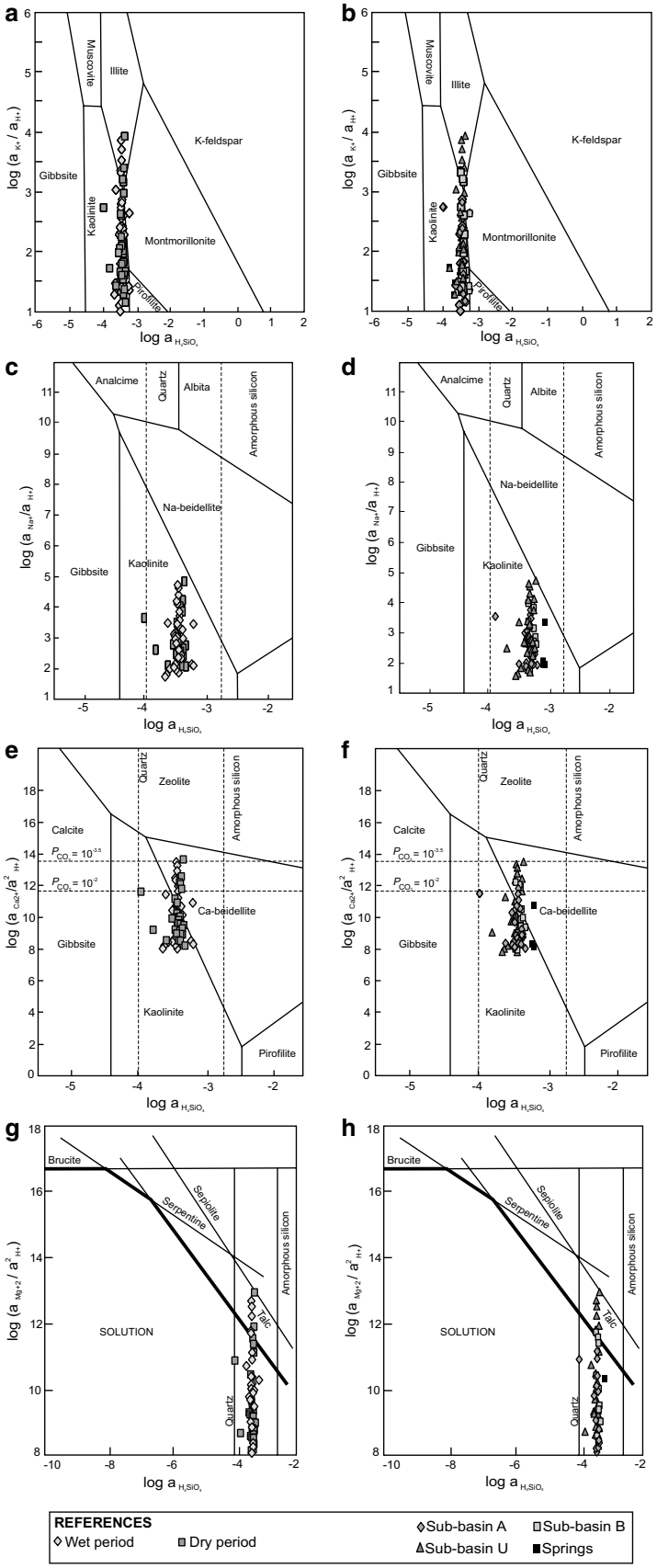

Fig. 3 Mineral stability diagrams of the systems: **a** and **b** $K_2O–Al_2O_3–SiO_2–H_2O$. **c** and **d** $Na_2O–Al_2O_3–SiO_2–H_2O$. **e** and **f** $CaO–Al_2O_3–SiO_2–H_2O$. **g** and **h** $MgO–Al_2O_3–SiO_2–H_2O$. Samples are discriminated by climatic season (**a**, **c**, **e**, **g**) and by sub-basin (**b**, **d**, **f**, **h**)

The weathering signature

Several weathering indices have been defined in the literature (e.g., Depetris et al. 2014) to determine the intensity of chemical alteration processes. Most of them compare the concentration of an immobile element with several mobile elements in the solid residue left by weathering. However, weathering can also be the assessed using the dissolved phases. In this sense, the modified version (Boeglin et al. 1997; Boeglin and Probst 1998) of the weathering index RE initially proposed by Tardy (1971), uses the concentrations of different dissolved elements. RE was defined in surface waters that drain granitic and gneissic catchments, and is calculated in molar proportions as follows:

$$RE = (3K^{+} + 3Na^{+} + 2Ca^{2+} + 1.25Mg^{2+} - SiO_2)/(0.5K^{+} + 0.5Na^{+} + Ca^{2+} + 0.75Mg^{2+}) \quad (1)$$

The different coefficients used in the above equation depend on the major primary minerals of the country rock and correspond to an average granitic composition with feldspars and micas (Tardy 1971). If RE = 0, the dominant weathering product is gibbsite; if RE = 2, the formation of kaolinite prevails; and if RE = 4, smectite is the most common weathering product. The mean RE value obtained for *La Trucha* is 2.48, which represents the monosiallitization weathering process and the corresponding kaolinite formation. The main channel (sub-basin U) exhibits a mean RE slightly higher (2.57) than the sub-basin A (mean RE = 2.3), indicating a tendency to the bisiallitization process (i.e., formation of smectites) toward the mouth.

Ternary diagrams are also extensively used tools in the literature to evaluate the extent of chemical weathering. Although most of them analyze the alteration in regoliths, Douglas (2006) proposed a ternary diagram using the molar proportions of the major cations of the dissolved phase. The weathering products of quartz, calcite and biotite plot at the apices, and the position of plagioclase weathering products is based on a plagioclase Ca–Na ratio of 0.3 reported by Ferry (1992).

Waters of *La Trucha* cluster around the transformation of plagioclase to kaolinite (Fig. 4), as it is expected in a granitic domain. Furthermore, a seasonal control on the catchment chemistry can be recognized. During the wet season, waters reflect the weathering of plagioclase in the basin, whereas during the dry season, waters also exhibit the chemical signature of the weathering of biotite and, to a lesser extent, of calcite (Fig. 4).

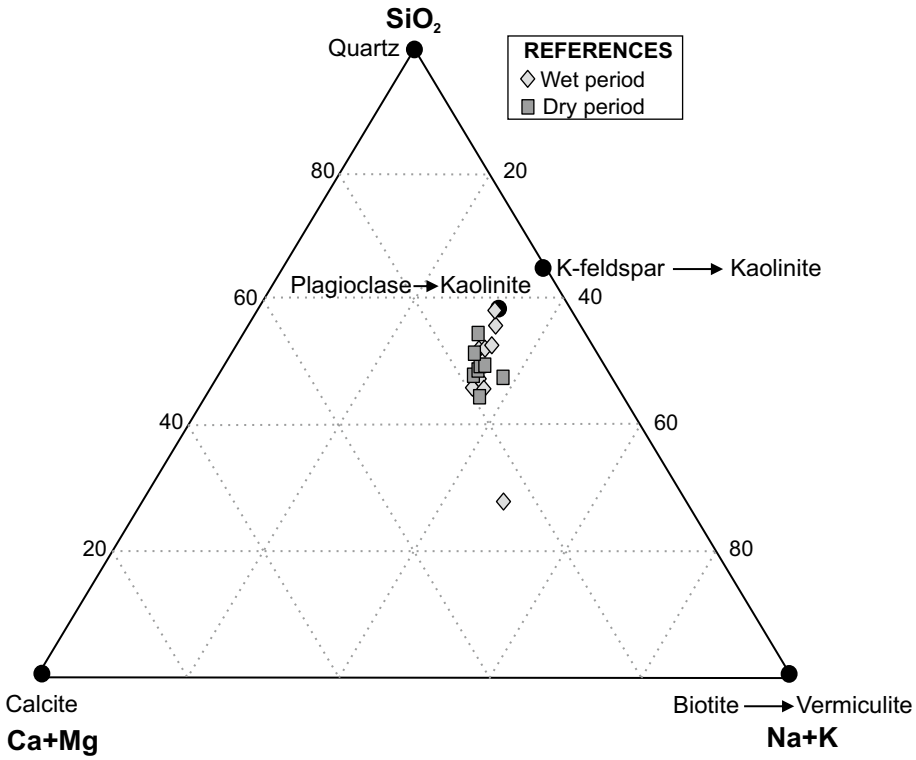

Fig. 4 Ternary diagram SiO_2–Ca + Mg–Na + K for waters from *La Trucha* drainage basin, discriminated by climatic season

Inverse models

The inverse geochemical modeling performed with the PHREEQC software was used to analyze the control of relief and climate on the incongruent dissolution of silicate minerals in the *La Trucha* drainage basin. Samples collected in June (models 1_{Jun}, 2_{Jun}, 3_{Jun} and 4_{Jun}) and March (models 1_{Mar}, 2_{Mar}, 3_{Mar} and 4_{Mar}), corresponding to the dry and wet seasons, respectively, were used to perform the modeling (Fig. 2). Stream discharge varies between 15 and 25 L s^{-1} during the dry season, and it may increase tenfold during the wet season (Martínez et al. 2016). The detailed results of the modeling runs are presented in Table 3.

Figure 5 shows the total quantities of dissolved and precipitated phases, separated by model and climatic season. It can be seen that the exchange that occurs between rainfall and the rocks/sediments of the basin have a strong impact on the surface water chemistry (i.e., model 1), which is about one order of magnitude higher than in the other models. For this reason, Fig. 6 shows the same results but only for models 2, 3 and 4, in order to better analyze the differences between them. In Fig. 6a, all the mineral and gaseous (CO_2) phases were considered. Both dissolution and precipitation are more intense during baseflow conditions, accounting for 2.57×10^{-4} mmol kg^{-1} H_2O for the dissolved phases and 2.76×10^{-4} mmol kg^{-1} H_2O for the precipitated phases when models 2, 3 and 4 are considered. Conversely, during the wet

Table 3 Selected PHREEQC inverse models: transferred dissolved and precipitated phases during wet (Mar) and dry (Jun) seasons

	Model 1_{Mar}		Model 2_{Mar}		Model 3_{Mar}		Model 4_{Mar}	
Phase	mmol kg^{-1} H_2O	%	mmol kg^{-1} H_2O	%	mmol kg^{-1} H_2O	%	mmol kg^{-1} H_2O	%
Biotite	1.51E−05	1.8	2.64E−06	2.4			6.05E−06	3.2
Carbon dioxide	3.18E−04	38.6	−5.95E−05	−53.2	3.56E−05	59.3	−9.49E−06	−5.0
Fluorite	3.33E−05	4.0	6.10E−06	5.5	2.35E−06	3.9	1.91E−05	10.0
Gypsum			8.94E−07	0.8	1.75E−06	2.9		
Illite	−1.76E−04	−21.4	−1.52E−05	−13.6	−1.29E−07	−0.2	−6.61E−05	−34.8
Kaolinite	−6.66E−05	−8.1					−1.41E−05	−7.4
K-feldspar								
K-mica	8.81E−05	10.7	8.79E−06	7.9			4.49E−05	23.7
Oligoclase	8.68E−05	10.5	2.28E−06	2.0			1.36E−05	7.1
Calcite	−3.87E−05	−4.7	1.63E−05	14.6	−1.64E−05	−27.4	−9.71E−06	−5.1
Pure water								
Halite					3.70E−06	6.2	6.87E−06	3.6
Total dissolved	5.41E−04	65.7	3.70E−05	33.1	4.34E−05	72.4	9.05E−05	47.7
Total precipitated	−2.82E−04	−34.2	−7.47E−05	−66.9	−1.66E−05	−27.6	−9.94E−05	−52.3
	Model 1_{Jun}		Model 2_{Jun}		Model 3_{Jun}		Model 4_{Jun}	
Biotite	1.55E−05	1.5	5.20E−06	1.7	2.13E−06	1.3		
Carbon dioxide	5.81E−04	56.9	−1.72E−04	−56.9	1.27E−04	76.7	4.12E−05	64.3
Fluorite	1.05E−05	1.0	2.26E−05	7.5	−5.67E−06	−3.4	−1.21E−05	−18.9
Gypsum	3.72E−07	0.0	2.46E−06	0.8			−2.37E−06	−3.7
Illite	−1.64E−04	−16.1	−3.95E−05	−13.1	−1.63E−05	−9.9	−9.95E−07	−1.6
Kaolinite	−7.02E−05	−6.9	−8.58E−06	−2.8				
K-feldspar								
K-mica	8.30E−05	8.1	2.06E−05	6.8	9.08E−06	5.5	6.89E−07	1.1
Oligoclase	8.47E−05	8.3	1.38E−05	4.6	2.67E−06	1.6		
Calcite	3.90E−06	0.4	−1.79E−05	−5.9	2.69E−06	1.6	6.74E−06	10.5
Pure water								
Halite	8.49E−06	0.8						
Total dissolved	7.87E−04	77.1	6.46E−05	21.3	1.43E−04	86.7	4.86E−05	75.8
Total precipitated	−2.34E−04	−22.9	−2.38E−04	−78.7	−2.20E−05	−13.3	−1.55E−05	−24.2

% represents the transferred amount for each phase divided by the total transferred amount (i.e., the sum of the values of all phases except water) expressed as a percentage

Positive values indicate dissolution, whereas negative values denote precipitation

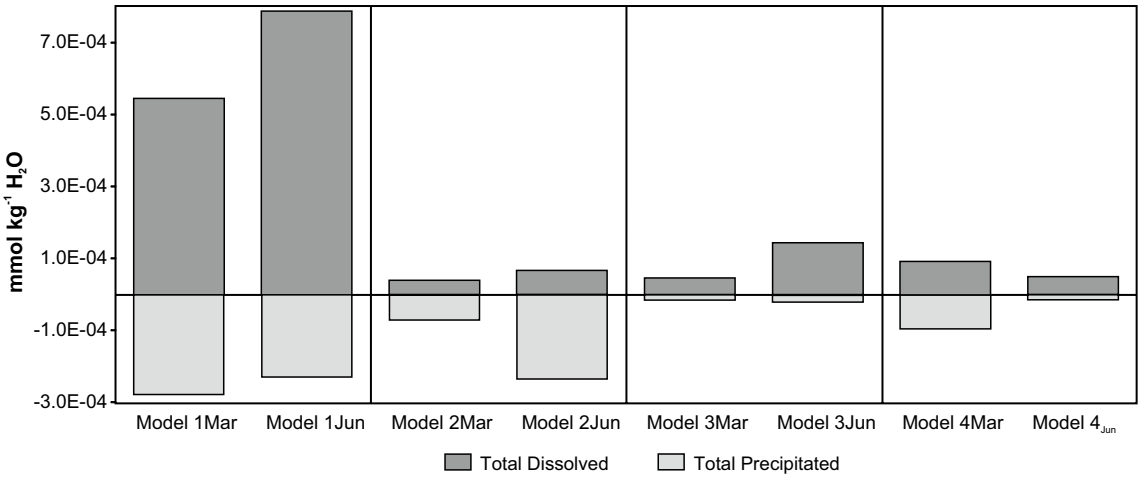

Fig. 5 Total transferred dissolved and precipitated phases during wet (Mar) and dry (Jun) seasons for each model

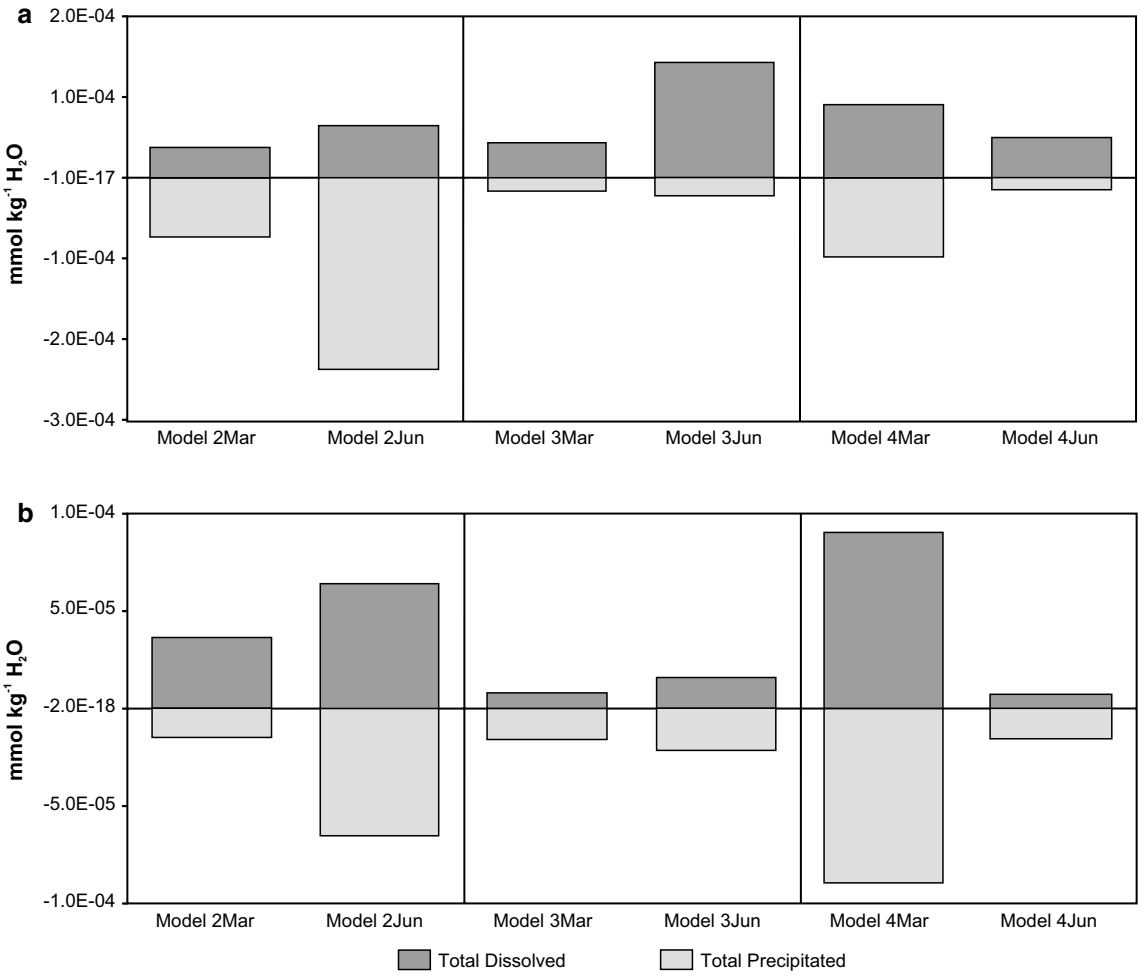

Fig. 6 Total transferred dissolved and precipitated phases during wet (Mar) and dry (Jun) seasons for models 2, 3 and 4. **a** Considering mineral and gaseous (CO_2) phases. **b** Considering only mineral phases

season, the amounts of the different phases that are dissolved or precipitated during the reactions decrease, with values of 1.71×10^{-4} mmol kg^{-1} H_2O and 1.91×10^{-4} mmol kg^{-1} H_2O, respectively. However, when different stream reaches (i.e., models) are analyzed separately, this general climatic pattern is not observed. For instance, in the lower basin (slopes ~ 7%) the larger dissolutions and precipitations take place during the wet season, whereas in the middle stretch (slopes ~ 2%), the dissolutions are higher in the dry season (Fig. 6a). The noticeable dominance of precipitated phases in the upper basin (i.e., model 2_{Jun}) during the dry season can be attributed to the CO_2 efflux (Fig. 6a).

The impact of CO_2 in surface water chemistry is more evident when only the mineral phases are considered (Fig. 6b). In this case, the total mineral dissolution (i.e., considering models 2, 3 and 4) is greater during the wet season. The lower basin (i.e., model 4_{Mar}) supplies greater amounts of dissolved phases during the wet season, whereas in the upper basin (i.e., model 2_{Jun}) the dissolution occurs mainly during the dry season (Fig. 6b). However, in this last stretch, the proportion of dissolved phases decreases compared to Fig. 6a, as the CO_2 evasion significantly contributes to this process.

The main transformations that explain the chemical evolution of surface waters are the dissolution of muscovite and oligoclase, and to a lesser extent of biotite, calcite and fluorite, and the precipitation of kaolinite and illite. Besides, depending on the climatic season and the analyzed stretch, CO_2, calcite and fluorite can dissolved or precipitate.

Figure 7 shows the percentages of mmol kg^{-1} H_2O of each mineral and gaseous species transferred in models 2, 3 and 4. Model 1 is excluded from the analysis to avoid misinterpretations caused by differences in orders of magnitude. It can be seen that K-feldspar and water do not explain the chemical changes that occur in the system, even though K-feldspar is abundant in the *Achala* Batholith. CO_2 is the dominant phase in the models, implying that carbon exchange at *La Trucha* drainage basin is significant. As it was stated by Martínez et al. (2016), in mountainous watersheds dominated by first- and second-order streams is common the degasification of spring waters that reach the main channel. The ambient temperature, biological activity, and rainfall are important factors that control the seasonality of CO_2 concentrations. In the case of *La Trucha*, the groundwater inflow, which generally shows higher CO_2 concentrations due to weathering processes and the in situ respiration of organisms present in soil (Schulte et al. 2011), constitutes an important source of CO_2. CO_2 constitutes 66% of the exchanged phases during the dry season and 39% during the wet season (Martínez et al. 2016). This is caused by the fact that during the dry season, springs are the major water suppliers to the main channel, and even though the CO_2 concentrations are lower during this period, the impact on the transferred phases is higher. This gaseous component is eliminated from the solution during both seasons (i.e., wet and dry) in the upper basin (i.e., models 2_{Mar} and 2_{Jun}), whereas in the middle stretch (i.e., models 3_{Mar} and 3_{Jun}), where the slopes are less steep, CO_2 is dissolved in both seasons. In the lower basin, CO_2 is eliminated in the wet season (i.e., model 4_{Mar}) and dissolved in the dry period (i.e., model 4_{Jun}).

The dissolution of muscovite, which is the main source of K^+, occurs mainly in the lower basin (i.e., model 4_{Mar}) during the wet season, whereas during the dry season muscovite is preferentially hydrolyzed at the headwaters (i.e., model 2_{Jun}) (Fig. 7). A similar behavior is observed for oligoclase (Fig. 7).

Fluorite, which partly explains the F^- concentration in the waters, exhibits a different behavior depending on the climatic season. It is preferentially dissolved during the wet season all along the drainage basin and its concentration is apparently higher where slopes are steeper (Fig. 7). In contrast, during the dry season, fluorite is only dissolved in the upper basin (i.e., model 2_{Jun}), whereas it appears to precipitate in the middle and lower stretches (i.e., models 3_{Jun} and 4_{Jun}) (Fig. 7).

Conversely to other mineral phases, calcite is dissolved mainly during the dry season (Fig. 7). During the wet season, it is dissolved in the upper basin (i.e., model 2_{Mar}) and precipitates in the middle and lower stretches (i.e., models 3_{Mar} and 4_{Mar}), whereas in the dry season it precipitates in the headwaters (i.e., model 2_{Jun}) and it is dissolved with greater intensity toward the outflow (Fig. 7).

Illite is the phase that better explains mineral precipitation at *La Trucha* drainage basin and it also shows a different behavior depending on the climatic season (Fig. 7). During the wet season, it precipitates mainly in the lower basin (i.e., model 4_{Mar}), while in the dry season this process preferentially occurs in the headwaters (i.e., model 2_{Jun}) and decreases more than one order of magnitude toward the outflow (Fig. 7).

When the CO_2 is not considered, it can be seen that the largest percentages of illite precipitation and dissolution of muscovite occur in the middle stretch (i.e., model 3), where the slopes are less steep (~ 2%) (Fig. 7).

Summary and concluding comments

La Trucha drainage basin is a small (~ 1.9 km^2), mountainous (~ 1300 m a.s.l.), relatively steep granitic drainage basin (i.e., the overall mean slope is ~ 5% although there are some considerably steeper – ~ 25% – stretches). It is representative of hundreds of second-order drainage basins in the *Achala* Batholith. This contribution is an integral part of an ongoing study (Campodonico et al. 2014; Martínez et al. 2016) which seeks to reach a detailed picture on the weathering occurring

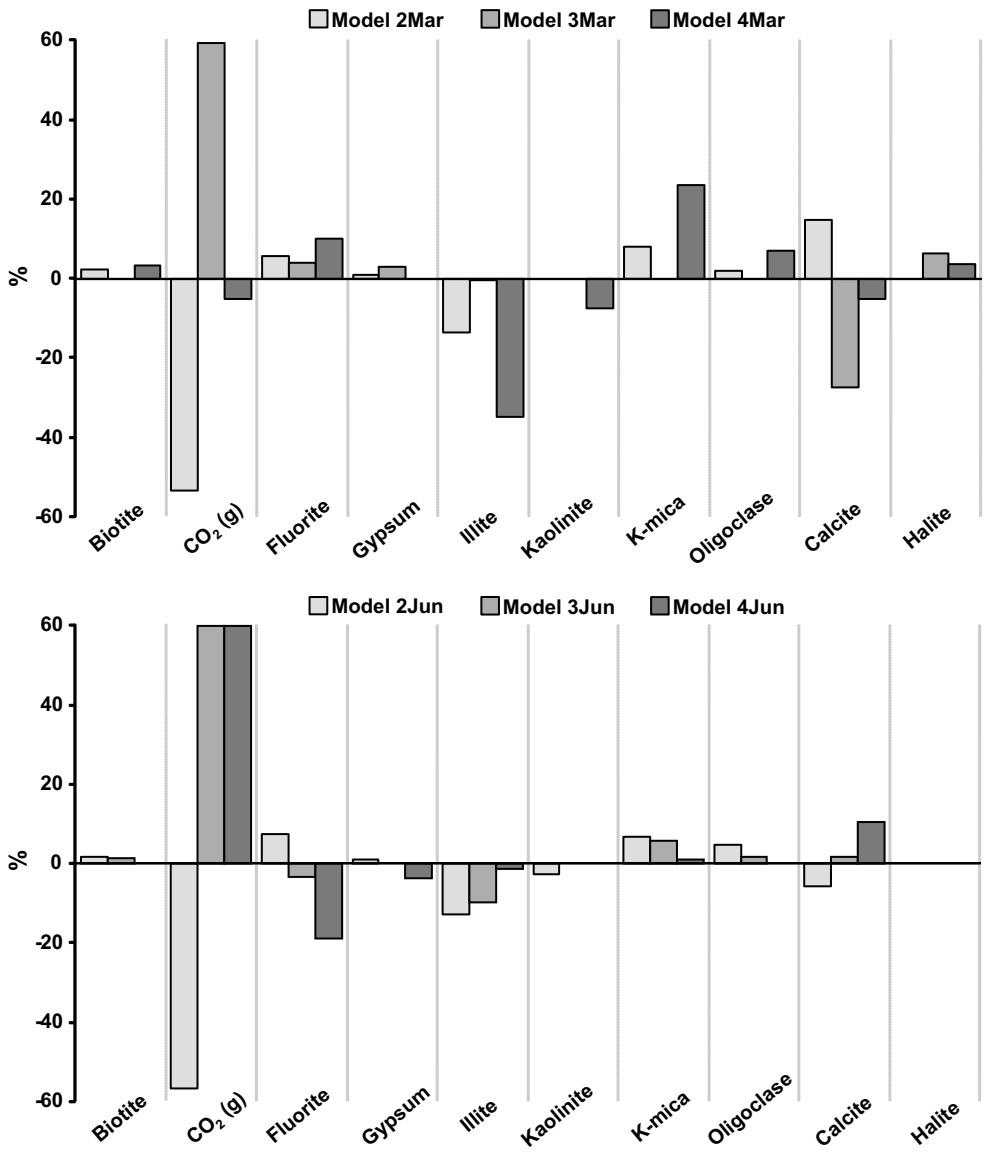

Fig. 7 PHREEQC inverse modeling results in percentages of mmol kg^{-1} H_2O of each mineral and gaseous species transferred in models 2, 3 and 4 during wet (Mar) and dry (Jun) seasons. Positive values are for dissolved phases and negative values are for precipitated ones

in the large intrusive body placed in the *Sierras Pampeanas* of Córdoba, Argentina. Moreover, mountains are increasingly looked upon in the context of global change and in this contribution we seek to expand the growing world data base on mountain systems (e.g., http://mri.scnatweb.ch).

Clearly subjected to a *weathering-limited* denudation regime—i.e., material is removed faster than it is produced by weathering- the remaining coarse- and fine-grained regolith has shown slight geochemical differences with the country rock (Campodonico et al. 2014). Significant erosion and sediment transport mainly happens during torrential rain events, hindering the assessment of weathering intensity following the traditional approach (i.e., identifying relative material gains and losses in the mineral phases). Therefore, the dissolved phases were analyzed to expand the insight on the nature of chemical weathering.

Surface waters at *La Trucha* were almost neutral or slightly alkaline (pH = 7.24 ± 0.79), and the mean total dissolved solids were 24.92 ± 5.14 mg L^{-1}. The mean alkalinity in surface waters—mostly accounted for HCO_3^- concentrations—was 349.67 ± 70.22 µeq L^{-1}. Surface waters classify as *dilute* or *very dilute* ($750 < T\Sigma^+ < 185$ µeq L^{-1}) water types and at the headwaters depict the chemical signature of rainfall.

In the stability diagram for the system K_2O–Al_2O_3–SiO_2–H_2O, samples fall within the kaolinite stability field. The absence of significant changes in the silicic acid concentration suggests that the main

source of K^+ is most likely muscovite, which liberates K^+, consumes H^+, and does not liberate H_4SiO_4 to the solution during its conversion to kaolinite. In the case of the $Na_2O–Al_2O_3–SiO_2–H_2O$ system, samples also plot in the kaolinite stability field, although a greater spread is perceived during the wet season when the concentration of Na^+ increases. Kaolinite and, to a lesser extent Ca-beidellite, are stable phases in the $CaO–Al_2O_3–SiO_2–H_2O$ system, being the latter more stable during the wet season. The $MgO–Al_2O_3–SiO_2–H_2O$ system crosses over the amorphous silica limit. The samples collected in the stream's main stem plot within the talc [$Mg_3Si_4O_{10}(OH)_2$] stability field, mostly during the wet season.

The other approach followed to probe into the nature of weathering was the RE index recommended by Tardy (1971). The mean RE value obtained for *La Trucha* is 2.48, which corresponds to kaolinite formation. The main channel exhibits a slightly higher index (2.57), suggesting a trend to the formation of smectites toward the mouth.

Ternary diagrams are also used extensively to appraise the degree of chemical weathering in different environments. As expected in granitic domains, the waters of *La Trucha* point to the transformation of plagioclase to kaolinite as the major process. Remarkably, during the rainy season, *La Trucha*'s water chemistry reveals the weathering of plagioclase, whereas it suggests the weathering of biotite and, somewhat less obvious, calcite, during the dry season (austral winter).

The final pathway followed in this methodological comparison was inverse modeling by means of the PHREEQC code to simulate chemical reactions occurring during the hydrolysis or dissolution of mineral phases. The inverse models propose the hydrolysis of silicates (e.g., feldspar, muscovite), the dissolution/precipitation of calcite, and the selective formation of clay minerals (e.g., illite, kaolinite). Particularly significant is the already underlined (Martínez et al. 2016) major role played by CO_2, which is in agreement with the results shown for first- and second-order streams in the USA. (Butman and Raymond 2011). However, the most important output surely is the proposition that small river geochemistry is responsive to seasons and behaves in each one in a diverse geochemical fashion, in coherency with the results obtained by Douglas (2006) at the White River of Vermont (U.S.A.).

Acknowledgements This research was funded by the Universidad Nacional de Córdoba (SECYT) and by Argentina's Consejo Nacional de Investigaciones Científicas y Técnicas (PIP N° 112-200801-03160 CONICET). The authors wish to acknowledge the personnel of *La Domanda* inn for their assistance during fieldwork. We thank three anonymous reviewers and the Editor for their constructive comments.

References

Bland W, Rolls D (1998) Weathering. An introduction to the scientific principles. Arnold, London

Boeglin JL, Probst JL (1998) Physical and chemical weathering rates and CO_2 consumption in a tropical lateritic environment: the upper Niger basin. Chem Geol 148:137–156

Boeglin JL, Mortatti J, Tardy Y (1997) Erosion Chimique et Mécanique sur le bassin amont du Niger (Guiné, Mali). Bilan Géochimique de l'altération en millieu tropical. C R Acad Sci, Paris 325:185–191

Bonalumi A, Martino RD, Sfragulla J, Baldo EG, Zarco J, Carignano CA, Tauber A, Kraemer P, Escayola M, Cabanillas A, Juri E, Torres B (1998) Hoja geológica 3166-IV, 1:250.000, Villa Dolores. Instituto de Geología y Recursos Minerales, SEGEMAR, Argentina. Bulletin 250

Butman D, Raymond PA (2011) Significant efflux of carbon dioxide from streams and rivers in the United States. Nat Geos. https://doi.org/10.1038/NGEO1294

Campodonico VA, Martínez JO, Verdecchia SO, Pasquini AI, Depetris PJ (2014) Weathering assessment in the *Achala* Batholith of the *Sierra de Comechingones*, Córdoba, Central Argentina. I: Granite-regolith fractionation. Catena 123:121–134

Capitanelli RG (1979) Geomorfología. In: Vázquez JB et al (eds) Geografía física de la Provincia de Córdoba. Boldt, Córdoba

Carson MA, Kirkby NJ (1972) Hillslope form and processes. Cambridge University Press, Cambridge

Dahlquist JA, Alasino PH, Bello C (2014) Devonian F-rich peraluminous A-type magmatism in the proto-Andean foreland (Sierras Pampeanas, Argentina): geochemical constraints and petrogenesis from the western central region of the *Achala* batholiths. Miner Pet 108:391–417

Depetris PJ, Pasquini AI, Lecomte KL (2014) Weathering and the riverine denudation of continents. Springer briefs in earth system sciences. Springer, Dordrecht

Douglas TA (2006) Seasonality of bedrock weathering chemistry and CO_2 consumption in a small watershed, the White River, Vermont. Chem Geol 231:236–251

Eaton AD, Clesceri LS, Greenberg AE (1995) Standard methods for the examination of water and wastewater. A.P.H.A./A.W.W.A./W.E.F, Washington DC

Faure G (1998) Principles and applications of geochemistry, 2nd edn. Prentice Hall, Upper Saddle River

Ferry JM (1992) Regional metamorphism of the Waits River Formation, eastern Vermont; delineation of a new type of giant metamorphic hydrothermal system. J Pet 33:45–94

Frings P, Clymans W, Fontorbe G, Gray W, Chakrapani G, Conley D, De La Rocha C (2015) Silicate weathering in the Ganges alluvial plain. Earth Planet Sci Lett 427:136–148

Hamdan J, Burnham CP (1996) The contribution of nutrients from parent material in three deeply weathered soils of Peninsula Malaysia. Geoderma 74:219–233

Harnois L (1988) The CIW index: a new chemical index of weathering. Sed Geol 55:319–322

Horton RE (1945) Erosional development of streams and their drainage basins. Hydrophysical approach to quantitative morphology. Geol Soc Am Bull 56:275–370

Isacks BL (1988) Uplift of the central Andean plateau and bending of the Bolivian orocline. J Geophys Res 93(B4):3211–3231

Lecomte KL, Pasquini AI, Depetris PJ (2005) Mineral weathering in a semiarid mountain river: its assessment through PHREEQC inverse modeling. Aquat Geochem 11:173–194

Lecomte KL, García MG, Fórmica SM, Depetris PJ (2009) Influence of geomorphological variables on mountainous stream water

chemistry (Sierras Pampeanas, Córdoba, Argentina). Geomorphology 110:195–202
Li Z, Tainosho Y, Shiraishi K, Owada M (2003) Chemical characteristics of fluorine-bearing biotite of early Paleozoic plutonic rocks from the Sor Rondane Mountains, East Antarctica. Geochem J 37:145–161
Lira R, Kirschbaum AM (1990) Geochemical evolution of granites from the *Achala* Batholith of the Sierras Pampeanas, Argentina. Geol Soc Am Spec Pap 241:67–76
Martínez JO, Campodonico VA, Fórmica SM, Depetris PJ (2016) Weathering assessment in the *Achala* Batholith of the *Sierra de Comechingones*, Córdoba, Central Argentina. II: major hydrochemical characteristics and carbon dynamics. Environ Earth Sci 75:554–572
Meybeck M (2005) Global occurrence of major elements in rivers. In: Drever JL (ed) Surface and ground water, weathering and soils. Elsevier, Amsterdam, pp 207–223
Nesbitt HW, Young GM (1982) Early Proterozoic climates and plate motions inferred from major element chemistry of lutites. Nature 299(5885):715–717
Nicolli H, Bundschuh J, Garcia J, Falcón C, Jean J (2010) Sources and controls for the mobility of arsenic in oxidizing groundwaters from loess-type sediments in arid/semi-arid dry climates—evidence from the Chaco-Pampean plain (Argentina). Water Res 44:5589–5604
Oliva P, Viers J, Dupré B (2003) Chemical weathering in granitic environments. Chem Geol 202:225–256
Parkhurst DL, Appelo CA (2013) Description of input and examples for PHREEQC version 3—a computer program for speciation, batch-reaction, one-dimensional transport, and inverse geochemical calculations. U.S. Geological Survey Techniques and Methods, book 6, Chap. A43
Pasquini AI, Lecomte KL, Depetris PJ (2004) Geoquímica de ríos de montaña en las Sierras Pampeanas: II. El río Los Reartes, Sierra de Comechingones, Provincia de Córdoba Argentina. Rev Asoc Geol Arg 59(1):129–140
Pasquini AI, Lecomte KL, Piovano EL, Depetris PJ (2006) Recent rainfall and runoff variability in central Argentina. Quat Int 158:127–139
Pasquini AI, Campodonico VA, Rouzaut S, Giampaoli V (2017) Geochemistry of a soil catena developed from loess deposits in a semiarid environment, Sierra Chica de Córdoba, central Argentina. Geoderma 295:53–68
Rapela CW, Baldo EG, Pankhurst RJ, Fanning CM (2008) The devonian *Achala* Batholith of the Sierras Pampeanas: F-rich, aluminous A-type granites. In: Proceedings of VI South American symposium on isotope geology, pp 1–8
Rouzaut S, Orgeira MJ (2017) Influence of volcanic glass on the magnetic signal of different paleosols in Córdoba, Argentina. Stud Geophys Geod 61:361–384
Schulte P, van Geldern R, Freitag H, AjazKarim A, Négrel P, Petelet-Giraud E, Probst A, Probst J-L, Telmer K, Veizer J, Barth JAC (2011) Applications of stable water and carbon isotopes in watershed research: weathering, carbon cycling, and water balances. Earth Sci Rev 10:20–31
Siegesmund S, Steenken A, Martino RD, Wemmer K, López de Luchi MG, Frei R, Presnyakov S, Guereschi AB (2010) Time constrains on the tectonic evolution of the Eastern Sierras Pampeanas (central Argentina). Int J Earth Sci 99:1199–1226
Strahler AN (1952) Hypsometric (area altitude) analysis of erosional topology. Geol Soc Am Bull 63:117–1142
Tardy Y (1971) Characterization of the principal weathering types by the geochemistry of waters form some European and African crystalline rocks. Chem Geol 7:253–271
Wohl E (2010) Mountain rivers revisited. American Geophysical Union, Washington DC